Taylor & Francis
Taylor & Francis Group

Evanescent waves in the magnetic field of an electric dipole

HENK F. ARNOLDUS*

Department of Physics and Astronomy, Mississippi State University,
P.O. Drawer 5167, Mississippi State, Mississippi, 39762-5167, USA

The magnetic field of radiation emitted by an electric dipole contains travelling and evanescent waves when represented as an angular spectrum. The evanescent waves decay exponentially away from the xy-plane, and will therefore not contribute to the detectable radiation in the far field, in general. It is well known, however, that in a small region around the z-axis the evanescent waves of the electric field do end up in the far zone. We have studied the corresponding magnetic evanescent waves, and we have found that the evanescent waves of the magnetic field do not contribute to the far zone in the neighbourhood of the z-axis. When considering the neighbourhood of the xy-plane, it appears that both the electric and magnetic evanescent waves end up in the far field, and the travelling and evanescent waves contribute equally to the radiation in the far zone. Close to the dipole the radiation field diverges, and we have shown that this is entirely due to the evanescent waves.

1. Introduction

Evanescent waves play a major role in near-field optics [1]. When a nanometre-size sample is illuminated with visible light, it will reflect travelling and evanescent waves. A detector of macroscopic size in the far field can only detect the travelling waves, since the evanescent waves die out over a distance of about a wavelength from the source. As a result, the spatial imaging resolution of a far field detector is limited to spatial variations in the sample of about a wavelength. Nevertheless, information on the finer structures of the sample is still present in the scattered light, but this information is carried by the evanescent waves. It has long been recognized that in order to build a microscope with sub-wavelength resolution, one has to measure the evanescent waves as well [2, 3]. This has led to the design of scanning near-field optical microscopes [4–10], in which a small fibre tip is moved over the sample, collecting the scattered light. In a different approach, light is sent through the fibre and the radiation emerging from its tip illuminates the sample. Since the aperture (opening of the tip) is sub-wavelength, the light contains evanescent waves due to diffraction [11, 12]. In such a setup, the sample is positioned on a hemispherical lens, which collects the light. Due to refraction at the surface of the lens, all travelling light ends up in a cone around the normal, and this cone has an opening angle equal to the critical angle of total internal reflection of the lens–air interface. Evanescent waves, radiated by the sample, can be converted into travelling waves at the interface,

---

*E-mail: arnoldus@ra.msstate.edu

provided their wavelength is not too short, and they are transmitted under an angle larger than the critical angle. In this way, part of the evanescent waves can be measured in the far field, improving the resolution of the image [13–20].

As mentioned above, evanescent waves can be detected in the far field after converting them into travelling waves by means of refraction at an interface. In a recent series of papers [21–24] it was shown that evanescent waves can also survive in the far field, without conversion into travelling waves first, for a specific direction of observation. The concept of evanescent waves originates in the angular spectrum representation of a radiation field. For this representation we need a reference surface, taken to be the xy-plane. A plane wave of the form $\exp{(i\boldsymbol{K} \cdot \boldsymbol{r})}$ has wave vector $\boldsymbol{K}$, and if $\boldsymbol{K}$ is real this is an ordinary travelling wave, propagating in the direction of this wave vector. In the angular spectrum representation, also waves with wave vectors with an imaginary z-component appear, and these are the evanescent waves. They decay exponentially away from the xy-plane, while still travelling along the xy-plane (the x- and y-components of $\boldsymbol{K}$ are real). One then easily assumes that since these waves die out exponentially in the positive and negative z-directions, they will not contribute to the radiation field far away from the source. In the quoted references, however, it was shown that there is a cylindrical region around the z-axis, with a diameter of about a wavelength, in which the evanescent waves survive in the far field, e.g., they decay as $\sim 1/r$, with r the distance to the source. Each evanescent wave decays exponentially in the z-direction, but the superposition of all evanescent waves decays as $1/r$. More recently it was shown [25, 26] that the evanescent waves also survive in the far field in a slab containing the xy-plane.

In theoretical investigations concerning the evanescent waves, one exclusively considers the electric component of the radiation field, with the idea that since the electric and magnetic field determine each other uniquely through Maxwell's equations, there is no need to consider the magnetic field separately. In this paper we shall consider the radiation field of an electric dipole, and focus our attention on the magnetic part. It will turn out that the evanescent part of the magnetic field behaves quite differently than the corresponding electric part.

2. The dipole field

We consider an electric dipole, located at the origin of coordinates, and oscillating harmonically with angular frequency ω. The time-dependent dipole moment is $\boldsymbol{d}(t) = \mathrm{Re}\,[\boldsymbol{d}\exp(-i\omega t)]$ with $\boldsymbol{d}$ an arbitrary complex-valued vector. The electric field is written as $\boldsymbol{E}(\boldsymbol{r}, t) = \mathrm{Re}\,[\boldsymbol{E}(\boldsymbol{r})\exp(-i\omega t)]$, with $\boldsymbol{E}(\boldsymbol{r})$ the complex amplitude, and similarly for the magnetic field $\boldsymbol{B}(\boldsymbol{r}, t)$. We shall adopt dimensionless coordinates throughout, with $1/k_o$ as the unit of measurement, where $k_o = \omega/c$ is the wave number. A field point $\boldsymbol{r}$ is then represented by $\boldsymbol{q} = k_o\boldsymbol{r}$, and $q = k_o r$ is the dimensionless distance to the origin. The electric field of the dipole is then most compactly given by

$$\boldsymbol{E}(\boldsymbol{r}) = \frac{k_o^3}{4\pi\varepsilon_o}\boldsymbol{\chi}(\boldsymbol{q}) \cdot \boldsymbol{d}, \tag{1}$$

with $\chi(q)$ the dimensionless Green's tensor [27, 28], defined as

$$\chi(q) = -\frac{4\pi}{3}\delta(q)\mathbf{I} + \left(\mathbf{I} + \frac{1}{k_o^2}\nabla\nabla\right)\frac{e^{iq}}{q}. \tag{2}$$

Here, $\delta(q) = \delta(r)/k_o^3$ is the dimensionless delta function and $\mathbf{I}$ is the unit tensor. After evaluating the derivatives we obtain

$$\chi(q) = -\frac{4\pi}{3}\delta(q)\mathbf{I} + (\mathbf{I} - 3\hat{q}\hat{q})\left(i - \frac{1}{q}\right)\frac{e^{iq}}{q^2} + (\mathbf{I} - \hat{q}\hat{q})\frac{e^{iq}}{q}, \tag{3}$$

with $\hat{q} = \hat{r}$. We see from equation (1) that all spatial dependence of the electric field is contained in the Green's tensor $\chi(q)$, and from equation (3) we observe the four distinctive parts: the first term is a delta function, which only gives a contribution inside the dipole, and this is called the self field. The other terms are $\mathcal{O}(q^{-3})$, $\mathcal{O}(q^{-2})$ and $\mathcal{O}(q^{-1})$, which are the near-, middle-, and far field, respectively.

The magnetic field can be written in a similar way as

$$\mathbf{B}(r) = \frac{i}{c}\frac{k_o^3}{4\pi\varepsilon_o}\eta(q) \times \mathbf{d}, \tag{4}$$

where the vector $\eta(q)$ is defined as

$$\eta(q) = -\frac{1}{k_o}\nabla\frac{e^{iq}}{q}, \tag{5}$$

and this is

$$\eta(q) = \hat{q}\left(\frac{1}{q} - i\right)\frac{e^{iq}}{q}. \tag{6}$$

We shall refer to $\eta(q)$ as the Green's vector since it serves the same purpose as the Green's tensor for the electric field. It should be noted, though, that $\eta(q)$ is not a Green's function in the usual sense. On the other hand, it is possible [29] to write the solution for $\mathbf{B}(r)$ in a form identical to equation (1) with a true Green's tensor and a dyadic product with $\mathbf{d}$ rather than a cross product, but that seems an unnecessary complication for the problem at hand. We notice that the magnetic field Green's vector has $\mathcal{O}(q^{-2})$ and $\mathcal{O}(q^{-1})$ terms only, in contrast to the Green's tensor for the electric field, which has additional self-field and near-field terms.

3. Angular spectrum representation

The function $\exp(iq)/q$ is the Green's function of the scalar wave equation, apart from an overall constant k_o. Weyl's representation of this function is [30, 31]

$$\frac{e^{iq}}{q} = \frac{i}{2\pi k_o}\int d^2k_{\parallel}\frac{1}{\beta}e^{i\mathbf{K}\cdot\mathbf{r}}, \tag{7}$$

where the wave vector $\mathbf{K}$ is given by

$$\mathbf{K} = \mathbf{k}_{\parallel} + \beta\,\text{sgn}(z)\mathbf{e}_z, \tag{8}$$

H. F. Arnoldus

and parameter β is defined as

$$\beta = \begin{cases} \sqrt{k_o^2 - k_\parallel^2}, & k_\parallel < k_o \\ i\sqrt{k_\parallel^2 - k_o^2}, & k_\parallel > k_o \end{cases}. \tag{9}$$

Representation (7) is commonly referred to as the angular spectrum representation of the scalar Green's function. Since $\beta^2 = k_o^2 - k_\parallel^2$, we see that $K = k_o$, and therefore each partial wave $\exp(i\boldsymbol{K} \cdot \boldsymbol{r})$ in equation (7) has the same wave number k_o. The parallel part of $\boldsymbol{K}$ with respect to the xy-plane is $\boldsymbol{k}_\parallel$, and the integration in equation (7) runs over the entire $\boldsymbol{k}_\parallel$-plane. For a given $\boldsymbol{k}_\parallel$, with magnitude $k_\parallel$, parameter β is real for $k_\parallel < k_o$, and therefore the z-component of $\boldsymbol{K}$ is real in this case. This situation corresponds to a travelling wave $\exp(i\boldsymbol{K} \cdot \boldsymbol{r})$, with $\boldsymbol{K}$ as the wave vector. Since β is positive we have $\text{sgn}(K_z) = \text{sgn}(z)$, and therefore the direction of propagation is away from the xy-plane, as illustrated in figure 1. For $k_\parallel > k_o$, parameter β is positive imaginary, and this corresponds to an evanescent wave which decays in the positive and negative z-directions. Since $\boldsymbol{k}_\parallel$ is real, the wave travels along the xy-plane in the $\boldsymbol{k}_\parallel$ direction, as shown schematically in figure 1. For these waves we have $k_\parallel > k_o$, indicating that the wavelength of the propagating component is smaller than an optical wavelength $(2\pi)/k_o$. It is this feature of the evanescent waves that opens the possibility of imaging an object on a sub-wavelength scale.

We now substitute the representation (7) into the right-hand side of equation (5) and move the operator ∇ under the integral. Taking the derivatives then yields the angular spectrum representation of the Green's vector

$$\boldsymbol{\eta}(\boldsymbol{q}) = \frac{1}{2\pi k_o^2} \int d^2 \boldsymbol{k}_\parallel \frac{1}{\beta} \boldsymbol{K} \, e^{i\boldsymbol{K} \cdot \boldsymbol{r}}, \tag{10}$$
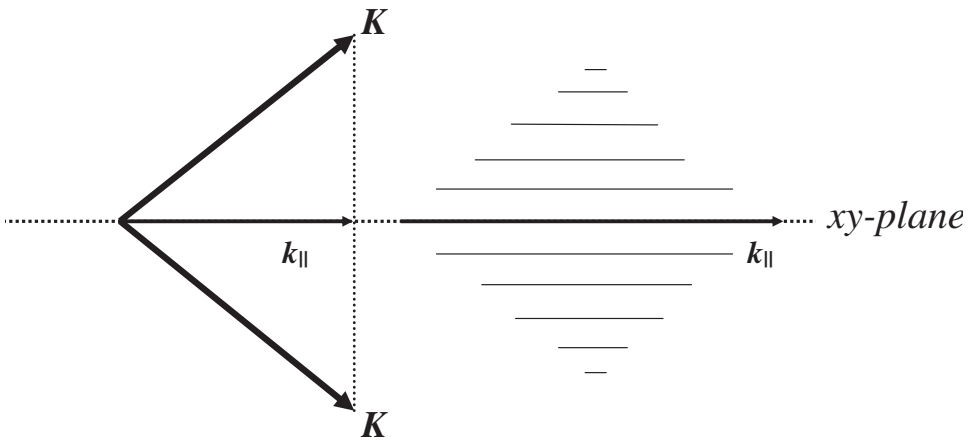
Figure 1. The two types of waves in the angular spectrum. For a given $\boldsymbol{k}_\parallel$ the wave vector is $\boldsymbol{K}$. When the z-component of $\boldsymbol{K}$ is real, the wave is travelling and on each side of the xy-plane it travels away from the xy-plane as shown on the left. When the z-component is imaginary the wave is evanescent, and decays away from the xy-plane, as shown on the right. Since $\boldsymbol{k}_\parallel$ is real, the wave travels along the xy-plane.

and with equation (4) this gives the angular spectrum representation of the magnetic field of an electric dipole:

$$B(r) = \frac{i\omega\mu_o}{8\pi^2} \int d^2k_{||} \frac{1}{\beta}(K \times d)e^{iK \cdot r}. \tag{11}$$

Clearly, $B(r)$ is a superposition of travelling and evanescent waves. The integration region $k_{||} < k_o$ is a disk in the $k_{||}$-plane, and the integral over this disk is a superposition of travelling waves. The integral over the remainder of the $k_{||}$-plane contains the evanescent waves. In this fashion, $B(r)$ splits naturally in a travelling part and an evanescent part. Since the entire spatial dependence of $B(r)$ is contained in the Green's vector $\eta(q)$, it is sufficient to consider the travelling and evanescent parts of this vector field. We write

$$\eta(q) = \eta(q)^{tr} + \eta(q)^{ev}, \tag{12}$$

in obvious notation.

4. Integration over $k_{||}$ and dimensionless variables

In order to study the angular spectrum representation (10) of $\eta(q)$ we shall adopt cylinder coordinates (ρ, ϕ, z) for a field point. For a given field point r, the radial and tangential unit vectors are $e_\rho = e_x \cos\phi + e_y \sin\phi$ and $e_\phi = -e_x \sin\phi + e_y \cos\phi$, respectively, so that $r = \rho e_\rho + z e_z$. For the integration over the $k_{||}$-plane we use the coordinate system shown in figure 2. The $\tilde{x}$- and $\tilde{y}$-axes are chosen to coincide with the radial and tangential unit vectors for the given field point, and then we use polar coordinates $(k_{||}, \tilde{\phi})$ in this $k_{||}$-plane. We furthermore introduce the dimensionless coordinates $\bar{\rho} = k_o\rho$ and $\bar{z} = k_o z$ in configuration space and the dimensionless coordinate $\alpha = k_{||}/k_o$ in the $k_{||}$-plane. We also define

$$\bar{\beta} = \frac{\beta}{k_o} = \sqrt{1 - \alpha^2}, \tag{13}$$

and it is understood that $\bar{\beta}$ is positive imaginary for $\alpha > 1$, as in equation (9). We then have $K = \alpha k_o(e_\rho \cos\tilde{\phi} + e_\phi \sin\tilde{\phi}) + k_o\bar{\beta}\,\text{sgn}(\bar{z})e_z$ and with $d^2k_{||} = k_o^2\alpha\,d\alpha\,d\tilde{\phi}$ we obtain

$$\eta(q) = \frac{1}{2\pi} \int_0^\infty d\alpha \frac{\alpha}{\bar{\beta}} e^{i\bar{\beta}|\bar{z}|} \int_0^{2\pi} d\tilde{\phi} \, [\alpha(e_\rho \cos\tilde{\phi} + e_\phi \sin\tilde{\phi}) + \bar{\beta}\,\text{sgn}(\bar{z})e_z]e^{i\alpha\bar{\rho}\cos\tilde{\phi}}. \tag{14}$$

The travelling part of $\eta(q)$ then follows from restricting the range of integration over α to $0 \le \alpha < 1$, and $\eta(q)^{ev}$ is given by equation (14) with the lower limit of integration replaced by $\alpha = 1$.

An interesting conclusion can be drawn immediately from equation (14). Let us consider the value of $\eta(q)^{tr}$ for $q \to 0$. Then both exponentials in the integrand disappear, and the integrals over $\cos\tilde{\phi}$ and $\sin\tilde{\phi}$ vanish. The remaining integral is elementary, with result

$$\eta(0)^{tr} = \frac{1}{2}\,\text{sgn}(\bar{z})e_z. \tag{15}$$

Apparently, the value of the travelling part is finite at the origin, whereas $\eta(q)$ itself is singular. Therefore, all singular behaviour of the magnetic field near the origin can only be due to the evanescent waves. This shows that indeed the evanescent waves
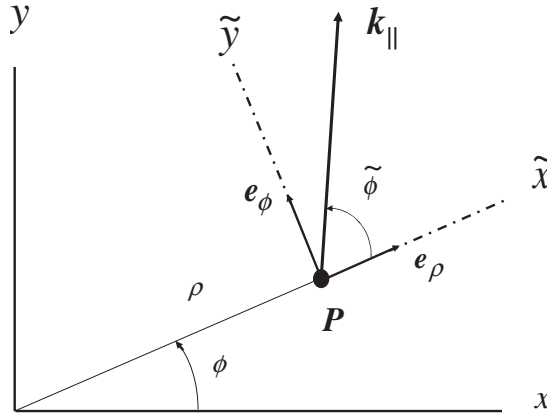
Figure 2. Point P is the projection of a field point $\mathbf{r}$ onto the xy-plane, and this point is taken as the origin of the $\mathbf{k}_\parallel$-plane. The diagram shows the coordinate system used in the $\mathbf{k}_\parallel$-plane.

dominate the field near the location of the source. We also notice that $\boldsymbol{\eta}(0)^{tr}$ is discontinuous across the xy-plane. The corresponding result for the Green's tensor of the electric field is [24]

$$\boldsymbol{\chi}(0)^{tr} = \frac{2}{3} i \, \mathbf{I}, \tag{16}$$

which is also finite.

5. Auxiliary functions

The integrals over $\tilde{\phi}$ in equation (14) lead to Bessel functions:

$$\int_0^{2\pi} d\tilde{\phi} \, \cos \tilde{\phi} \, e^{i\alpha\bar{\rho}\cos\tilde{\phi}} = 2\pi i J_1(\alpha\bar{\rho}), \tag{17}$$

$$\int_0^{2\pi} d\tilde{\phi} \, \sin \tilde{\phi} \, e^{i\alpha\bar{\rho}\cos\tilde{\phi}} = 0, \tag{18}$$

$$\int_0^{2\pi} d\tilde{\phi} \, e^{i\alpha\bar{\rho}\cos\tilde{\phi}} = 2\pi J_0(\alpha\bar{\rho}). \tag{19}$$

We can then write the Green's vector as

$$\boldsymbol{\eta}(\mathbf{q}) = \operatorname{sgn}(\bar{z}) \mathbf{e}_z M_e(\mathbf{q}) + \mathbf{e}_\rho M_f(\mathbf{q}), \tag{20}$$

in terms of the auxiliary functions

$$M_e(\mathbf{q}) = \int_0^\infty d\alpha \, \alpha J_0(\alpha\bar{\rho}) e^{i\bar{\beta}|\bar{z}|}, \tag{21}$$

$$M_f(\mathbf{q}) = i \int_0^\infty d\alpha \, \frac{\alpha^2}{\bar{\beta}} J_1(\alpha\bar{\rho}) e^{i\bar{\beta}|\bar{z}|}. \tag{22}$$

The Green's tensor can be written in a similar way [32], involving four different auxiliary functions $M_a(\mathbf{q}), \ldots, M_d(\mathbf{q})$ with a similar appearance. It follows from equations (21) and (22) that these two functions are invariant under reflection in the xy-plane and under rotation around the z-axis.

On the other hand, $\boldsymbol{\eta}(\boldsymbol{q})$ is given by equation (6). The dimensionless cylinder coordinates $(\bar{\rho}, \phi, \bar{z})$ of a field point are related to the dimensionless spherical coordinates (q, θ, ϕ) by $\bar{\rho} = q \sin \theta$, $\bar{z} = q \cos \theta$, and the unit vector $\hat{\boldsymbol{q}}$ in equation (6) can be expressed as $\hat{\boldsymbol{q}} = \boldsymbol{e}_\rho \sin \theta + \boldsymbol{e}_z \cos \theta$. When we compare expressions (6) and (20), the $\boldsymbol{e}_\rho$ and $\boldsymbol{e}_z$ components must be the same, and this leads immediately to the result

$$M_e(\boldsymbol{q}) = \frac{|\bar{z}|}{q^2} \left(\frac{1}{q} - i \right) e^{iq}, \tag{23}$$

$$M_f(\boldsymbol{q}) = \frac{\bar{\rho}}{q^2} \left(\frac{1}{q} - i \right) e^{iq}. \tag{24}$$

From equations (23) and (24) we see that the two functions are related as

$$\bar{\rho} M_e(\boldsymbol{q}) = |\bar{z}| M_f(\boldsymbol{q}). \tag{25}$$

6. Evanescent and travelling parts

The evanescent part of the magnetic field is determined by the evanescent part of the Green's vector, which is

$$\boldsymbol{\eta}(\boldsymbol{q})^{ev} = \mathrm{sgn}(\bar{z}) \boldsymbol{e}_z M_e(\boldsymbol{q})^{ev} + \boldsymbol{e}_\rho M_f(\boldsymbol{q})^{ev}, \tag{26}$$

and here the evanescent parts of the auxiliary functions follow from replacing the lower limit of integration $\alpha = 0$ by $\alpha = 1$ in equations (21) and (22). Furthermore we have $\bar{\beta} = i(\alpha^2 - 1)^{1/2}$ in the evanescent region. The following theorem involving Bessel functions

$$|\bar{z}| \int_1^\infty d\alpha \frac{\alpha^{n+1}}{\sqrt{\alpha^2 - 1}} J_n(\alpha \bar{\rho}) e^{-|\bar{z}|\sqrt{\alpha^2 - 1}} = J_n(\bar{\rho}) + \bar{\rho} \int_1^\infty d\alpha \, \alpha^n J_{n-1}(\alpha \bar{\rho}) e^{-|\bar{z}|\sqrt{\alpha^2 - 1}}, \quad n = 0, 1, \ldots, \tag{27}$$

can be proved by setting

$$\frac{\alpha}{\sqrt{\alpha^2 - 1}} e^{-|\bar{z}|\sqrt{\alpha^2 - 1}} = -\frac{1}{|\bar{z}|} \frac{d}{d\alpha} e^{-|\bar{z}|\sqrt{\alpha^2 - 1}} \tag{28}$$

in the integrand on the left-hand side and a subsequent integration by parts. For the remaining integral we use $(x^n J_n(x))' = x^n J_{n-1}(x)$, and this proves the theorem. By setting $n = 1$, the theorem becomes

$$\bar{\rho} M_e(\boldsymbol{q})^{ev} = |\bar{z}| M_f(\boldsymbol{q})^{ev} - J_1(\bar{\rho}). \tag{29}$$

relating the evanescent parts of both functions. As compared to the corresponding relation (25) for the unsplit functions, we see that the splitting in a travelling and an evanescent part gives an additional Bessel function $J_1(\bar{\rho})$.

For further analysis it is useful to make the change of integration variable $u = (\alpha^2 - 1)^{1/2}$ in the integral representations. This gives

$$M_e(\boldsymbol{q})^{ev} = \int_0^\infty du\, u J_0(\bar{\rho}\sqrt{1 + u^2})e^{-u|\bar{z}|}, \tag{30}$$

$$M_f(\boldsymbol{q})^{ev} = \int_0^\infty du\,\sqrt{1 + u^2} J_1(\bar{\rho}\sqrt{1 + u^2})e^{-u|\bar{z}|}. \tag{31}$$

In the representation (22) for $M_f(\boldsymbol{q})$, the integrand has a singularity at $\alpha = 1$, since at this value we have $\bar{\beta} = 0$. After the change of variables, this singularity has disappeared, indicating that the original singularity is integrable, and therefore causes no problems. A second conclusion that can be drawn from equations (30) and (31) is that the evanescent parts of the auxiliary functions are real-valued. With equation (20) we then see that $\boldsymbol{\eta}(\boldsymbol{q})^{ev}$ is real, and therefore the imaginary part of $\boldsymbol{\eta}(\boldsymbol{q})$ only contains travelling waves. This also implies that only the real part of $\boldsymbol{\eta}(\boldsymbol{q})$ splits in a travelling and an evanescent part, and the same holds for the functions $M_e(\boldsymbol{q})$ and $M_f(\boldsymbol{q})$. From equations (23) and (24) we obtain

$$\text{Re}M_e(\boldsymbol{q}) = \frac{|\bar{z}|}{q^2}\left(\sin q + \frac{\cos q}{q}\right), \tag{32}$$

$$\text{Re}M_f(\boldsymbol{q}) = \frac{\bar{\rho}}{q^2}\left(\sin q + \frac{\cos q}{q}\right), \tag{33}$$

and these functions split as

$$\text{Re}M_k(\boldsymbol{q}) = M_k(\boldsymbol{q})^{ev} + \text{Re}M_k(\boldsymbol{q})^{tr}, \quad k = e, f. \tag{34}$$

Therefore, we know $M_k(\boldsymbol{q})^{ev}$ if we know $\text{Re}M_k(\boldsymbol{q})^{tr}$, and vice versa.

For the travelling parts of the auxiliary functions we only need to consider $\text{Re}M_k(\boldsymbol{q})^{tr}$, since the imaginary parts are simply the imaginary parts of equations (23) and (24). In order to obtain suitable integral representations, we limit the integration range to $0 \leq \alpha < 1$ in equations (21) and (22), set $u = (1 - \alpha^2)^{1/2}$ and take the real parts, which yields

$$\text{Re}M_e(\boldsymbol{q})^{tr} = \int_0^1 du\, u J_0(\bar{\rho}\sqrt{1 - u^2})\cos(u|\bar{z}|), \tag{35}$$

$$\text{Re}M_f(\boldsymbol{q})^{tr} = -\int_0^1 du\,\sqrt{1 - u^2} J_1(\bar{\rho}\sqrt{1 - u^2})\sin(u|\bar{z}|). \tag{36}$$

When we take the difference between equations (25) and (29) we find

$$\bar{\rho}M_e(\boldsymbol{q})^{tr} = |\bar{z}|M_f(\boldsymbol{q})^{tr} + J_1(\bar{\rho}). \tag{37}$$

7. The z-axis and the xy-plane

For a field point on the z-axis we have $\bar{\rho} = 0$ and $|\bar{z}| = q$, so that we have with equations (23) and (24)

$$M_e(\boldsymbol{q}) = \left(\frac{1}{q} - i\right)\frac{e^{iq}}{q}, \tag{38}$$

$$M_f(\boldsymbol{q}) = 0. \tag{39}$$

With $J_0(0) = 1$ the integral in equation (30) is elementary and with $J_1(0) = 0$ the integral in equation (31) vanishes. This yields for the evanescent parts of the auxiliary functions

$$M_e(\boldsymbol{q})^{ev} = \frac{1}{q^2}, \tag{40}$$

$$M_f(\boldsymbol{q})^{ev} = 0. \tag{41}$$

and the Green's vector becomes

$$\boldsymbol{\eta}(\boldsymbol{q})^{ev} = \frac{1}{q^2} \operatorname{sgn}(\bar{z}) \boldsymbol{e}_z. \tag{42}$$

The most important observation here is that $\boldsymbol{\eta}(\boldsymbol{q})^{ev} = \mathcal{O}(q^{-2})$, which is of the middle field type. Therefore, the evanescent waves in the magnetic field do not survive in the far field along the z-axis. This in contrast to the evanescent waves in the electric field for which we have [24]

$$\boldsymbol{\chi}(\boldsymbol{q})^{ev} = \frac{1}{2q}(\mathbf{I} + \boldsymbol{e}_z\boldsymbol{e}_z) - \frac{1}{q^3}(\mathbf{I} - 3\boldsymbol{e}_z\boldsymbol{e}_z), \tag{43}$$

which is $\mathcal{O}(q^{-1})$. We come to the remarkable conclusion that even though the electric and magnetic fields determine each other uniquely, the evanescent magnetic field vanishes along the z-axis whereas the evanescent electric field does not.

For the travelling part along the z-axis we find from equations (35) and (36)

$$\operatorname{Re}M_e(\boldsymbol{q})^{tr} = \frac{1}{q}\left(\sin q + \frac{\cos q}{q}\right) - \frac{1}{q^2}, \tag{44}$$

$$\operatorname{Re}M_f(\boldsymbol{q})^{tr} = 0. \tag{45}$$

The first term on the right-hand side of equation (44) is just $\operatorname{Re}M_e(\boldsymbol{q})$, equation (32). We therefore conclude that due to the splitting in travelling and evanescent waves, the travelling waves get an extra term $-1/q^2$, which is just the negative of $M_e(\boldsymbol{q})^{ev}$.

For a field point in the xy-plane we have $|\bar{z}| = 0$ and $\bar{\rho} = q$ and we find from equations (23) and (24)

$$M_e(\boldsymbol{q}) = 0, \tag{46}$$

$$M_f(\boldsymbol{q}) = \left(\frac{1}{q} - i\right)\frac{e^{iq}}{q}. \tag{47}$$

We now consider the travelling part first. When we set $|\bar{z}| = 0$ in equation (35) the remaining integral is cumbersome. Instead we consider equation (37), from which we obtain

$$\operatorname{Re}M_e(\boldsymbol{q})^{tr} = \frac{1}{q}J_1(q). \tag{48}$$

Since $\operatorname{Re}M_e(\boldsymbol{q}) = 0$, we find for the evanescent part

$$M_e(\boldsymbol{q})^{ev} = -\frac{1}{q}J_1(q). \tag{49}$$

Here we observe the interesting situation that a function which is identically zero splits in non-zero travelling and evanescent parts. We will get back to this in

section 13. Bessel functions are $\mathcal{O}(q^{-1/2})$ for q large, and therefore both $\text{Re}M_e(\boldsymbol{q})^{tr}$ and $M_e(\boldsymbol{q})^{ev}$ are $\mathcal{O}(q^{-3/2})$, and they do not end up in the far field.

From equation (36) with $|\bar{z}| = 0$ we find

$$\text{Re}M_f(\boldsymbol{q})^{tr} = 0, \tag{50}$$

which gives for the evanescent part with equation (32)

$$M_f(\boldsymbol{q})^{ev} = \frac{1}{q}\left(\sin q + \frac{\cos q}{q}\right). \tag{51}$$

This is $\mathcal{O}(q^{-1})$, so of the far field type. Apparently, along the xy-plane and in the far field, the real part of the Green's vector is pure evanescent. Since the imaginary part is travelling and $\mathcal{O}(q^{-1})$, we conclude that along the xy-plane the travelling and evanescent waves contribute equally to the magnetic far field. This behaviour is the same as for the electric field [24]. The evanescent part of the Green's vector in the far field is up to leading order

$$\boldsymbol{\eta}(\boldsymbol{q})^{ev} \approx \hat{\boldsymbol{q}}\,\frac{\sin q}{q}. \tag{52}$$

8. Asymptotic series for large $|\bar{z}|$

In order to study systematically the evanescent waves in the far field, we now derive an asymptotic expansion of the auxiliary functions for $|\bar{z}|$ large. In the integral representation (30) for $M_e(\boldsymbol{q})^{ev}$ we replace the Bessel function by its series expansion

$$J_n(x) = \sum_{k=0}^{\infty} \frac{(-1)^k}{k!(k+n)!}\left(\frac{x}{2}\right)^{2k+n}, \tag{53}$$

which gives

$$M_e(\boldsymbol{q})^{ev} = \sum_{k=0}^{\infty} \frac{(-1)^k}{(k!)^2}\left(\frac{\bar{\rho}}{2}\right)^{2k}\int_0^{\infty} du\, u(1+u^2)^k e^{-u|\bar{z}|}. \tag{54}$$

The integral on the right-hand side can be evaluated as

$$\int_0^{\infty} du\, u(1+u^2)^k e^{-u|\bar{z}|} = \sum_{\ell=0}^{k} \binom{k}{\ell}\frac{(2\ell+1)!}{|\bar{z}|^{2\ell+2}}. \tag{55}$$

We substitute this into equation (54), change the order of summation and set $n = k - \ell$ in the summation over k. The sum over n then has the appearance of a Bessel function, as in equation (53), and we obtain

$$M_e(\boldsymbol{q})^{ev} = \frac{1}{|\bar{z}|^2}\sum_{\ell=0}^{\infty} \frac{(2\ell+1)!}{\ell!}\left(-\frac{\bar{\rho}}{2\bar{z}^2}\right)^{\ell} J_\ell(\bar{\rho}). \tag{56}$$

In a similar way we find

$$M_f(\boldsymbol{q})^{ev} = -\frac{1}{|\bar{z}|}\sum_{\ell=0}^{\infty} \frac{(2\ell)!}{\ell!}\left(-\frac{\bar{\rho}}{2\bar{z}^2}\right)^{\ell} J_{\ell-1}(\bar{\rho}), \tag{57}$$

where we used that $J_{-1}(\bar{\rho}) = -J_1(\bar{\rho})$.

For a field point on the z-axis we have $\bar{\rho} = 0$, and since $J_\ell(0) = 0$ for $\ell \neq 0$ and $J_0(0) = 1$ the series solutions reduce to $M_e(\boldsymbol{q})^{ev} = 1/|\bar{z}|^2$ and $M_f(\boldsymbol{q})^{ev} = 0$, which is the exact solution for all points on the z-axis (equations (40) and (41)). Off the z-axis the series diverge, and they should be understood as an asymptotic series for $|\bar{z}|$ large, and with $\bar{\rho}$ fixed. The first few terms are

$$M_e(\boldsymbol{q})^{ev} = \frac{1}{|\bar{z}|^2} J_0(\bar{\rho}) + \mathcal{O}(|\bar{z}|^{-4}), \tag{58}$$

$$M_f(\boldsymbol{q})^{ev} = \frac{1}{|\bar{z}|} J_1(\bar{\rho}) + \frac{\bar{\rho}}{|\bar{z}|^3} J_0(\bar{\rho}) + \mathcal{O}(|\bar{z}|^{-5}). \tag{59}$$

Figure 3 shows the exact $M_f(\boldsymbol{q})^{ev}$, obtained by numerical integration, and the approximation by the first term on the right-hand side of equation (59). We see that for relatively small values of $\bar{z}$ the agreement is already excellent.

Let us now consider the dependence on the distance q to the origin. For $\bar{\rho}$ small, we found in the previous section that the Green's vector is $\mathcal{O}(q^{-2})$, and is given by equation (42). For $\bar{\rho}$ large, we can use the asymptotic form of the Bessel functions

$$J_n(\bar{\rho}) \approx \sqrt{\frac{2}{\pi\bar{\rho}}} \cos(\bar{\rho} - \frac{1}{2}n\pi - \frac{1}{4}\pi). \tag{60}$$

With $\bar{\rho} = q\sin\theta$ we see that the Bessel functions are $\mathcal{O}(q^{-1/2})$, and with $\bar{z} = q\cos\theta$ we find that the leading term in the auxiliary functions is the first term on the right-hand side of equation (59), which is $\mathcal{O}(q^{-3/2})$. The leading term in the Green's vector of the evanescent magnetic field is therefore

$$\boldsymbol{\eta}(\boldsymbol{q})^{ev} \approx \frac{1}{q^{3/2}} \frac{1}{|\cos\theta|} \sqrt{\frac{2}{\pi\sin\theta}} \sin(q\sin\theta - \pi/4)\boldsymbol{e}_\rho. \tag{61}$$

We conclude that near the z-axis the evanescent Green's vector is $\mathcal{O}(q^{-2})$, and this term comes from the first term on the right-hand side of equation (58), so from $M_e(\boldsymbol{q})^{ev}$. Off the z-axis, the evanescent field becomes $\mathcal{O}(q^{-3/2})$, due to the first term in the series for $M_f(\boldsymbol{q})^{ev}$. In both regions, the decay is faster than $\mathcal{O}(q^{-1})$, so there is no contribution to the far field. Also interesting is that the vector character changes from being proportional to $\boldsymbol{e}_z$ in equation (42) to being proportional to $\boldsymbol{e}_\rho$ in equation (61). For details of the transition between the two regions one has to retain the Bessel functions in the first terms on the right-hand sides of equations (58) and (59).

9. Uniform asymptotic approximation

The results in the previous section were derived from the asymptotic series for $|\bar{z}|$ large, and the conclusions do not extend all the way to field points near the xy-plane. This is most obvious from equation (61), where the right-hand side diverges for $\theta \rightarrow \pi/2$. In this section we shall obtain an asymptotic approximation which holds uniformly for all angles, ranging from $\theta = 0$ to $\theta = \pi$, and passing smoothly through the xy-plane. We start from the integral representations (30) and (31) for $M_e(\boldsymbol{q})^{ev}$
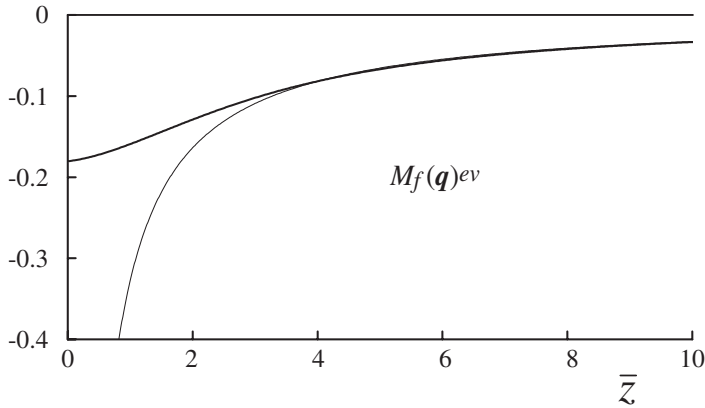
Figure 3. Function $M_f(\boldsymbol{q})^{ev}$ as a function of $\bar{z}$ for $\bar{\rho} = 5$. The thick line is the exact result and the thin line is the asymptotic approximation for large $\bar{z}$ with only the first term of the series used.

and $M_f(\boldsymbol{q})^{ev}$. Initially, we consider $\bar{\rho}$ large, so that we can replace the Bessel functions by their asymptotic form, given by equation (60) with $\bar{\rho} \to \bar{\rho}(1 + u^2)^{1/2}$. This gives

$$M_e(\boldsymbol{q})^{ev} \approx \sqrt{\frac{2}{\pi\bar{\rho}}} \operatorname{Re} e^{-i(\pi/4)(2n+1)} \int_0^\infty du \frac{u}{(1 + u^2)^{1/4}} e^{-u|\bar{z}|+i\bar{\rho}\sqrt{1+u^2}}, \qquad (62)$$

and a similar expression for $M_f(\boldsymbol{q})^{ev}$. We then set $\bar{\rho} = q\sin\theta$, $\bar{z} = q\cos\theta$, and consider the behaviour of these integrals for q large, θ fixed. It was recognized by Berry [25], who considered the scalar Green's function which has a similar integral representation, that these integrals have two critical points. On one hand there is the endpoint of integration $u = 0$, and on the other hand, the exponent has a saddle point at $u = -i|\cos\theta|$. When θ approaches $\pi/2$, the saddle point approaches the other critical point $u = 0$. Asymptotic approximations for such types of integrals can be made with Bleistein's method [33–35]. This method provides an approximation for the integral appearing on the right-hand side of equation (62), which holds near $\theta = \pi/2$ and smoothly connects to the region $\theta \neq \pi/2$. Due to the factor $\bar{\rho}^{-1/2}$ in front of the integral, the result can not be extended to include the z-axis as well in one formula. Recently, we modified Bleistein's method for integrals of the type given in equations (30) and (31), in such a way that the approximation also holds when the field point approaches the z-axis [26]. Instead of repeating this rather lengthy derivation, we shall simply give the result here.

First we introduce the universal function

$$N(\boldsymbol{q}) = -|\cos\theta|e^{iq}\left[\operatorname{erfc}(\xi) - \frac{1}{\xi\sqrt{\pi}}e^{-\xi^2}\right], \qquad (63)$$

which involves the parameter

$$\xi = (1 + i)\sqrt{\frac{1}{2}q(1 - \sin\theta)}, \qquad (64)$$

and the complementary error function of complex argument. This function can be written in the alternative form

$$N(\boldsymbol{q}) = \sqrt{\frac{1 + \sin\theta}{\pi q}} e^{i(\bar{\rho} - \pi/4)} - |\cos\theta| e^{iq} \mathrm{erfc}(\xi). \tag{65}$$

The asymptotic approximations are then found to be

$$M_e(\boldsymbol{q})^{ev} \approx -\frac{1}{q} \mathrm{Im} N(\boldsymbol{q}), \tag{66}$$

$$M_f(\boldsymbol{q})^{ev} \approx \frac{1}{|\bar{z}|} [J_1(\bar{\rho}) - \sin\theta \, \mathrm{Im} N(\boldsymbol{q})]. \tag{67}$$

We notice that only the imaginary part of $N(\boldsymbol{q})$ enters this result, whereas for the corresponding expressions for the auxiliary functions of the Green's tensor for the electric field only the real part of $N(\boldsymbol{q})$ was involved [26].

In order to see the significance of this result, let us first consider the behaviour of the function $N(\boldsymbol{q})$. For a point in the xy-plane we have $\theta = \pi/2$, and the function $N(\boldsymbol{q})$ becomes

$$N(\boldsymbol{q})_{\theta=\pi/2} = \sqrt{\frac{2}{\pi q}} e^{i(q - \pi/4)}, \tag{68}$$

as follows from equation (65). The most important point here is that this is $\mathcal{O}(q^{-1/2})$. Off the xy-plane we have $\theta \neq \pi/2$, and this makes ξ large if q is large. In this case we use expression (63) for $N(\boldsymbol{q})$ and we can approximate the complementary error function with its asymptotic expansion [36]:

$$\mathrm{erfc}(\xi) = \frac{1}{\xi\sqrt{\pi}} e^{-\xi^2} \left[1 + \sum_{n=1}^{\infty} (-1)^n \frac{1 \cdot 3 \cdot \cdots \cdot (2n-1)}{(2\xi^2)^n} \right]. \tag{69}$$

Interestingly, the first term is just the second term in square brackets in equation (63), and therefore $N(\boldsymbol{q})$ is $\mathcal{O}(\xi^{-3})$, which is $\mathcal{O}(q^{-3/2})$. The function $N(\boldsymbol{q})$ provides the smooth transition from the xy-plane into the region $\theta \neq \pi/2$, and the behaviour changes gradually from $\mathcal{O}(q^{-1/2})$ to $\mathcal{O}(q^{-3/2})$. Figure 4 shows the real and imaginary parts of $N(\boldsymbol{q})$ as a function of θ for $q = 32$.

The approximation to $M_e(\boldsymbol{q})^{ev}$, given by equation (66), is then seen to be $\mathcal{O}(q^{-3/2})$ near the xy-plane and $\mathcal{O}(q^{-5/2})$ off the xy-plane. Bleistein's method gives an accurate approximation up to order $q^{-3/2}$, so this approximation is only reliable near the xy-plane. The exact result in the xy-plane is given by equation (49), and with the approximation (60) for $J_1(q)$, we see that this is asymptotically equivalent to equation (66), given the value of $N(\boldsymbol{q})$ in equation (68).

More interesting is the approximation for $M_f(\boldsymbol{q})^{ev}$, equation (67). Off the xy-plane, $N(\boldsymbol{q})$ is $\mathcal{O}(q^{-3/2})$, and with $|\bar{z}| = q|\cos\theta|$ we find that the term with $N(\boldsymbol{q})$ gives an $\mathcal{O}(q^{-5/2})$ contribution, which is negligible compared to the term with the Bessel function, which is $\mathcal{O}(q^{-3/2})$. Therefore we might as well set

$$M_f(\boldsymbol{q})^{ev} \approx \frac{1}{|\bar{z}|} J_1(\bar{\rho}). \tag{70}$$

This is just the first term on the right-hand side of equation (59), which is the asymptotic approximation for large $|\bar{z}|$, and which is exact on the z-axis. When approaching the xy-plane, the function $N(\boldsymbol{q})$ becomes $\mathcal{O}(q^{-1/2})$, which is the same order as the Bessel function. In that case, both terms have to be retained. The result (67) is then an undetermined form for $\theta \to \pi/2$, if we replace $J_1(\bar{\rho})$ by its asymptotic form (60), and this case has to be considered with a limit. It can be shown that this limit is

$$M_f(\boldsymbol{q})^{ev} \approx \frac{\sin q}{q}, \tag{71}$$

which is asymptotically equivalent to the exact result (51). The picture that emerges is that on the z-axis the evanescent magnetic waves in the far field are negligible, meaning at most $\mathcal{O}(q^{-2})$. Off the z-axis, the function $M_f(\boldsymbol{q})^{ev}$ becomes $\mathcal{O}(q^{-3/2})$, with $M_e(\boldsymbol{q})^{ev}$ still negligible. When approaching the xy-plane, the function $M_e(\boldsymbol{q})^{ev}$ contributes as $\mathcal{O}(q^{-3/2})$, but now $M_f(\boldsymbol{q})^{ev}$ becomes $\mathcal{O}(q^{-1})$, which is a far field contribution. We conclude that the evanescent magnetic waves contribute to the far field in a region near the xy-plane, are $\mathcal{O}(q^{-3/2})$ off the xy-plane, and are negligible near the z-axis. The situation for the electric field is similar, except that when approaching the z-axis, the evanescent electric waves become $\mathcal{O}(q^{-1})$. The uniform asymptotic approximation, given by equations (66) and (67), then accounts for the smooth transition between the three regions of different behaviour. Figure 5 illustrates the accuracy of the approximation for $M_f(\boldsymbol{q})^{ev}$.

The conclusions from the previous paragraph can be quantified a little further. The transition between the $\mathcal{O}(q^{-1})$ and the $\mathcal{O}(q^{-3/2})$ behaviour is determined by the function $N(\boldsymbol{q})$. This function becomes $\mathcal{O}(q^{-3/2})$ when the argument of the complementary error function is large enough for the asymptotic expansion (69) to set in. This occurs at about $|\xi| \approx 1$, and with equation (64) this gives $q - \bar{\rho} \approx 1$. Since $q = (\bar{\rho}^2 + \bar{z}^2)^{1/2}$ and $|\bar{z}| \ll \bar{\rho}$, this is equivalent to $|\bar{z}|^2 \approx 2\bar{\rho}$. Therefore, given $\bar{\rho}$, there is a layer with a thickness of about $|\bar{z}| \sim \sqrt{\bar{\rho}}$ around the xy-plane, and inside this layer the evanescent waves end up in the far field. Although the thickness of this
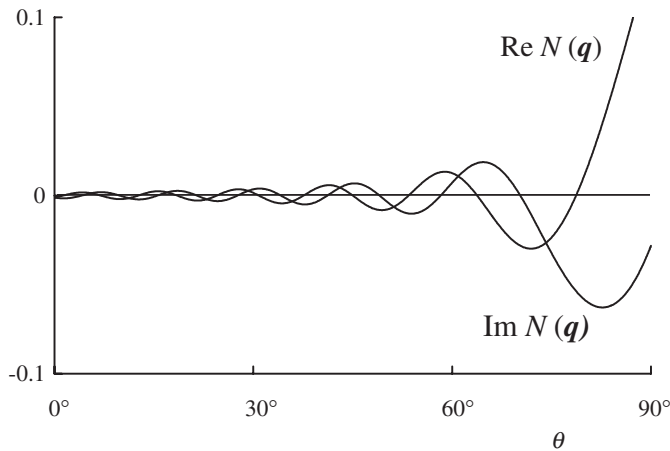
Figure 4.   Real and imaginary parts of $N(\boldsymbol{q})$ as a function of θ for $q = 32$.

layer grows indefinitely with the distance to the origin, the angular width of this layer is asymptotically zero.

10. Series expansion for small z

In section 8 we considered the evanescent waves of the magnetic field for $|\bar{z}|$ large, leading to asymptotic series for the auxiliary functions. We now consider the complementary case of $\bar{z}$ small, with $\bar{\rho}$ fixed. We start from the integral representations (35) and (36) for the real parts of the travelling parts. In equation (35) we replace the Bessel function $J_0(\bar{\rho}\sqrt{1 - u^2})$ by its series expansion (53) and we also expand $\cos(u|\bar{z}|)$ in its series representation for small argument. This yields the double series

$$\mathrm{Re}M_e(\boldsymbol{q})^{tr} = \sum_{k=0}^{\infty}\sum_{\ell=0}^{\infty}\frac{(-1)^{k+\ell}}{(k!)^2(2\ell)!}\left(\frac{\bar{\rho}}{2}\right)^{2k}|\bar{z}|^{2\ell}\int_0^1 du\,(1 - u^2)^k u^{2\ell+1}. \tag{72}$$

The integral on the right-hand side is

$$\int_0^1 du(1 - u^2)^k\,u^{2\ell+1} = \frac{k!\ell!}{2(k + \ell + 1)!}, \tag{73}$$

and when substituted into equation (72), the summation over k can be represented by a Bessel function. We then obtain the series expansion

$$\mathrm{Re}M_e(\boldsymbol{q})^{tr} = \frac{1}{\bar{\rho}}\sum_{\ell=0}^{\infty}\frac{\ell!}{(2\ell)!}\left(-\frac{2\bar{z}^2}{\bar{\rho}}\right)^{\ell}J_{\ell+1}(\bar{\rho}), \tag{74}$$

and in a similar way we find

$$\mathrm{Re}M_f(\boldsymbol{q})^{tr} = -\frac{|\bar{z}|}{\bar{\rho}}\sum_{\ell=0}^{\infty}\frac{\ell!}{(2\ell + 1)!}\left(-\frac{2\bar{z}^2}{\bar{\rho}}\right)^{\ell}J_{\ell+2}(\bar{\rho}). \tag{75}$$
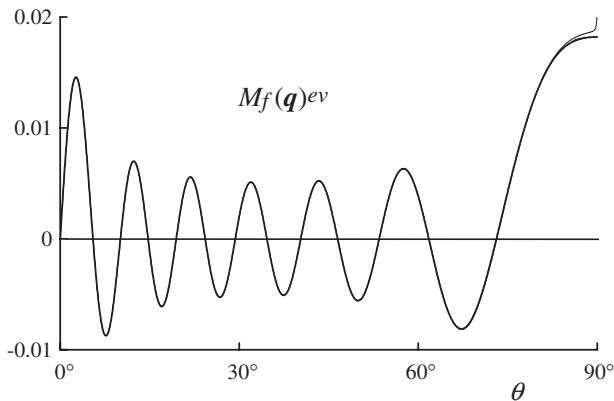
Figure 5. The thick line is the exact value of $M_f(\boldsymbol{q})^{ev}$ for $q = 40$, and the thin line is the uniform asymptotic approximation from equation (67). Except close to 90° the approximation appears perfect. The behaviour near 90° improves with increasing q.

This result has a remarkable resemblance with equations (56) and (57) for the asymptotic series for the evanescent parts. The difference is that now we have Taylor expansions in $\bar{z}$, for fixed $\bar{\rho}$, and the series converge for all $\bar{z}$. We also notice that for $\bar{z} = 0$ the results (74) and (75) reduce to equations (48) and (50), respectively, which were derived in an independent way. The evanescent parts near the xy-plane can now be found by taking the difference with equations (32) and (33). Figures 6 and 7 show the result of the series summation up to $\ell = 20$ for the travelling and evanescent parts, respectively. When more terms are included, numerical rounding becomes a problem, and one would have to go to double precision. Figure 7 complements figure 3, and we see that there is a considerable overlap between the range of applicability of the series expansion ($\bar{z} \lesssim 15$) and the asymptotic approximation ($\bar{z} \gtrsim 4$).

11. The near field

In section 9 we found a uniform asymptotic approximation for the evanescent magnetic waves in the far field (q large). In this section we shall consider the complementary situation of q small, which is the near field. In the previous section we obtained a series expansion in $\bar{z}$, which is useful for $\bar{z}$ small, although the series converges for all $\bar{z}$. The Taylor coefficients then became functions of $\bar{\rho}$. We shall now derive a series expansion in q, around $q = 0$, and such that the coefficients of the terms in the series become functions of the polar angle θ. To this end, we start from equations (74) and (75), in which we replace the Bessel functions by their series representation (53). We find for $\mathrm{Re}M_e(\boldsymbol{q})^{tr}$

$$\mathrm{Re}M_e(\boldsymbol{q})^{tr} = \frac{1}{\bar{\rho}} \sum_{\ell=0}^{\infty} \sum_{k=0}^{\infty} (-1)^{\ell+k} \frac{\ell!}{(2\ell)!k!(k+\ell+1)!} \bar{z}^{2\ell} \left(\frac{\bar{\rho}}{2}\right)^{2k+1}, \tag{76}$$

and a similar expression for $\mathrm{Re}M_f(\boldsymbol{q})^{tr}$. Then we rearrange the order of summation, similar as in the Cauchy product for a double series, set $\bar{\rho} = q\sin\theta$, $\bar{z} = q\cos\theta$, and collect the powers of q. This yields the series expansions in q

$$\mathrm{Re}M_e(\boldsymbol{q})^{tr} = \frac{1}{2} \sum_{n=0}^{\infty} Q_n(\theta) \frac{(-q^2/4)^n}{n!(n+1)!}, \tag{77}$$

$$\mathrm{Re}M_f(\boldsymbol{q})^{tr} = -\frac{1}{4} q^2 \sin\theta |\cos\theta| \sum_{n=0}^{\infty} P_n(\theta) \frac{(-q^2/4)^n}{n!(n+2)!}. \tag{78}$$

with coefficients that are functions of θ. These coefficient functions are defined by

$$P_n(\theta) = n! \sum_{k=0}^{n} \frac{k!}{(n-k)!(2k+1)!} (\sin^2\theta)^{n-k} (4\cos^2\theta)^k, \tag{79}$$

$$Q_n(\theta) = n! \sum_{k=0}^{n} \frac{k!}{(n-k)!(2k)!} (\sin^2\theta)^{n-k} (4\cos^2\theta)^k. \tag{80}$$

With $Q_0(\theta) = 1$ we find the values of the auxiliary functions at the origin of co-ordinates to be $\mathrm{Re}M_e(0)^{tr} = 1/2$, $\mathrm{Re}M_f(0)^{tr} = 0$, and this agrees with equation (15) for the travelling part of the Green's vector at the origin.
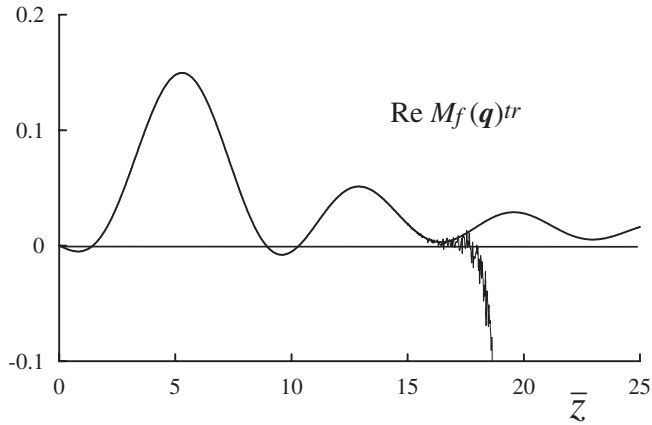
Figure 6. The graph shows the exact value of $\mathrm{Re}M_f(\boldsymbol{q})^{tr}$ and its approximation by the series with Bessel functions, equation (75), for $\bar{\rho} = 5$, and the series terminated at $\ell = 20$. The series approximation is accurate up to about $\bar{z} = 15$. When more terms are retained, the range can be increased, but one would have to go to double precision in order to avoid the noticeable rounding problems that are starting to set in.
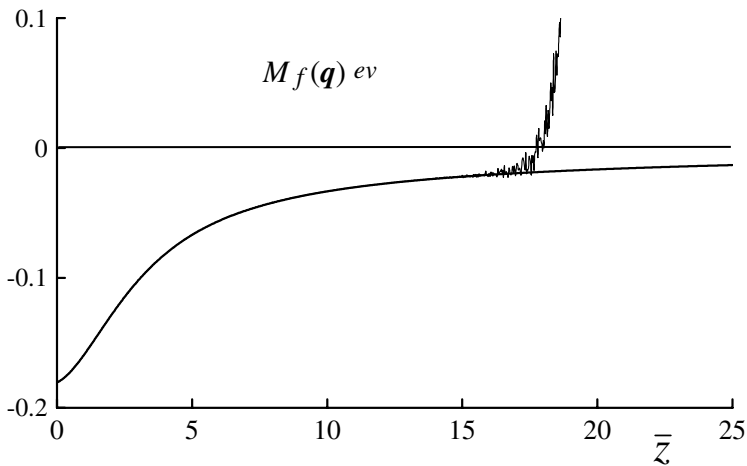
Figure 7. Exact value of $M_f(\boldsymbol{q})^{ev}$ and the result obtained from the series expansion of the corresponding travelling part, given by equation (75), for $\bar{\rho} = 5$. The series is summed up to $\ell = 20$.

In order to obtain the evanescent part near the origin, we use equation (34) in combination with the expressions for the unsplit functions $\mathrm{Re}M_k(\boldsymbol{q})$, given by equations (32) and (33). We expand the right-hand side of equation (32) in a series in q:

$$\mathrm{Re}M_e(\boldsymbol{q}) = |\cos\theta|\frac{1}{q^2} + |\cos\theta|\sum_{n=0}^{\infty}\frac{(-1)^n(2n+1)}{(2n+2)!}q^{2n}, \tag{81}$$

and similarly for the right-hand side of equation (33), and then we take the difference with the series in equations (77) and (78). This yields the series expansions of the evanescent parts

$$M_e(\boldsymbol{q})^{ev} = |\cos\theta|\frac{1}{q^2} + \frac{1}{2}\sum_{n=0}^{\infty} q_n(\theta)\frac{(-q^2/4)^n}{n!(n+1)!}, \tag{82}$$

$$M_f(\boldsymbol{q})^{ev} = \sin\theta\left(\frac{1}{q^2} + \frac{1}{2}\right) - \frac{1}{4}q^2\sin\theta\sum_{n=0}^{\infty} p_n(\theta)\frac{(-q^2/4)^n}{n!(n+2)!}. \tag{83}$$

which involve new coefficient functions $p_n(\theta)$ and $q_n(\theta)$. These new functions are related to the functions of the travelling parts as

$$p_n(\theta) = P_n(0) - |\cos\theta|P_n(\theta), \tag{84}$$

$$q_n(\theta) = |\cos\theta|Q_n(0) - Q_n(\theta). \tag{85}$$

The values of $P_n(\theta)$ and $Q_n(\theta)$ at $\theta = 0$ that appear here are given by

$$P_n(0) = \frac{4^n(n!)^2}{(2n+1)!}, \tag{86}$$

$$Q_n(0) = \frac{4^n(n!)^2}{(2n)!}, \tag{87}$$

as follows from equations (79) and (80) (only the $n = k$ terms contribute).

Equations (82) and (83) show that the singular behaviour of the magnetic evanescent waves near the origin is $\mathcal{O}(q^{-2})$. Since the travelling part is finite, we obtain for the total Green's vector, equation (20),

$$\boldsymbol{\eta}(\boldsymbol{q}) = \text{sgn}(\bar{z})\,\boldsymbol{e}_z\frac{1}{q^2}|\cos\theta| + \boldsymbol{e}_\rho\frac{1}{q^2}\sin\theta + \mathcal{O}(1), \tag{88}$$

and since $\text{sgn}(\bar{z}) = \text{sgn}(\cos\theta)$, this is

$$\boldsymbol{\eta}(\boldsymbol{q}) = \frac{1}{q^2}\hat{\boldsymbol{q}} + \mathcal{O}(1). \tag{89}$$

On the other hand, $\boldsymbol{\eta}(\boldsymbol{q})$ is given by equation (6), and when we expand the right-hand side in a series in q, we obtain the same first term as in equation (89). Here we have shown that this singular term is entirely due to the evanescent waves, which shows that indeed the evanescent waves dominate the near field.

12. Coefficient functions

The definitions (79) and (80) for $P_n(\theta)$ and $Q_n(\theta)$, respectively, are not very suitable for numerical evaluation, nor do they shed any light on the behaviour of these

functions. In this section we derive some interesting properties of these functions. To this end, we introduce the generating functions for $P_n(\theta)$ and $Q_n(\theta)$:

$$g_P(\theta; t) = \sum_{n=0}^{\infty} P_n(\theta) \frac{t^n}{n!}, \tag{90}$$

$$g_Q(\theta; t) = \sum_{n=0}^{\infty} Q_n(\theta) \frac{t^n}{n!}. \tag{91}$$

When we substitute the right-hand side of equation (79) into equation (90), the resulting expression has the form of a Cauchy product of a double series. We use Cauchy's theorem backwards, and write the result as a double series. This gives

$$g_P(\theta; t) = \sum_{k=0}^{\infty} \sum_{\ell=0}^{\infty} \frac{k!}{\ell!(2k+1)!} (t \sin^2 \theta)^{\ell} (4t \cos^2 \theta)^k. \tag{92}$$

Here the summation over ℓ gives an exponential, leading to

$$g_P(\theta; t) = e^{t \sin^2 \theta} \sum_{k=0}^{\infty} \frac{k!}{(2k+1)!} (4t \cos^2 \theta)^k. \tag{93}$$

The sum of this series can be expressed in terms of an error function [37], which yields

$$g_P(\theta; t) = \frac{1}{2 \cos \theta} \sqrt{\frac{\pi}{t}} e^t \operatorname{erf}(\sqrt{t} \cos \theta), \tag{94}$$

and in a similar way we obtain

$$g_Q(\theta; t) = e^{t \sin^2 \theta} + \cos \theta \sqrt{\pi t}\, e^t \operatorname{erf}(\sqrt{t} \cos \theta). \tag{95}$$

Next we use the series expansion for the error function to write $g_P(\theta; t)$ as

$$g_P(\theta; t) = \sum_{k=0}^{\infty} \frac{(-\cos^2 \theta)^k}{k!(2k+1)} (t^k e^t), \tag{96}$$

from which we can find $P_n(\theta)$ according to

$$P_n(\theta) = \left. \frac{d^n g_P(\theta; t)}{dt^n} \right|_{t=0}. \tag{97}$$

Carrying out the differentiation then gives the alternative expression for $P_n(\theta)$

$$P_n(\theta) = \sum_{k=0}^{n} \binom{n}{k} \frac{(-\cos^2 \theta)^k}{2k+1}. \tag{98}$$

With the same procedure for $Q_n(\theta)$ we obtain a similar series due to the error function in equation (95), and the first term on the right-hand side gives rise to an additional term. We find

$$Q_n(\theta) = (\sin \theta)^{2n} + 2n \cos^2 \theta P_{n-1}(\theta), \quad n = 1, 2, \ldots, \tag{99}$$

relating the functions $Q_n(\theta)$ to the functions $P_n(\theta)$. Then we set $\sin^2\theta = 1 - \cos^2\theta$, and combine the two terms, using equation (98) for $P_{n-1}(\theta)$, which gives

$$Q_n(\theta) = -\sum_{k=0}^{n} \binom{n}{k} \frac{(-\cos^2\theta)^k}{2k-1}, \tag{100}$$

as an alternative to equation (80).

Now we introduce the function

$$Y_n(x) = \sum_{k=0}^{n} \binom{n}{k} \frac{(-1)^k}{2k+1} x^{2k+1}, \tag{101}$$

and from equation (98) we see that $Y_n(\cos\theta) = \cos\theta P_n(\theta)$. It is easy to see that $Y_n(x)$ satisfies the differential equation

$$\frac{dY_n}{dx} = (1 - x^2)^n, \tag{102}$$

which can be integrated as

$$Y_n(x) = \int_0^x dt (1 - t^2)^n, \tag{103}$$

since $Y_n(0) = 0$. We write this as

$$Y_n(x) = Y_{n-1}(x) - \int_0^x dt\, t^2 (1 - t^2)^{n-1}, \tag{104}$$

and here we set $u(t) = (1 - t^2)^n$, from which $(1 - t^2)^{n-1} = (-2nt)^{-1} du/dt$. Integration by parts then gives a relation between $Y_n(x)$ and $Y_{n-1}(x)$, and when we substitute $x = \cos\theta$ we obtain the recursion relation for the coefficient functions

$$(2n+1)P_n(\theta) = 2nP_{n-1}(\theta) + (\sin^2\theta)^n, \quad n = 1, 2, \dots. \tag{105}$$

Since the functions $Q_n(\theta)$ are related to the functions $P_n(\theta)$, according to equation (99), this also implies a recursion relation between the functions $Q_n(\theta)$, and we find

$$(2n-1)Q_n(\theta) = 2nQ_{n-1}(\theta) - (\sin^2\theta)^n, \quad n = 1, 2, \dots. \tag{106}$$

With $P_0(\theta) = Q_0(\theta) = 1$ as initial values, these recursion relations provide a means to efficiently compute a large number of these functions. From equation (105) we readily deduce that the functions $P_n(\theta)$ are bounded as $0 < P_n(\theta) \le 1$. From equation (99) it follows that $Q_n(\theta) \le 1 + 2n$. Furthermore, by combining equations (99) and (105) we can derive the relation

$$Q_{n+1}(\theta) = Q_n(\theta) + \cos^2\theta\, P_n(\theta), \tag{107}$$

from which we conclude $Q_{n+1}(\theta) \ge Q_n(\theta)$. Since $Q_0(\theta) = 1$ we then find that the functions $Q_n(\theta)$ fall within the limits $1 \le Q_n(\theta) \le 1 + 2n$. Finally we notice the special values of $P_n(\pi/2) = Q_n(\pi/2) = 1$. Figure 8 shows the functions for $n = 3$.

The coefficient functions $p_n(\theta)$ and $q_n(\theta)$ are related to the functions $P_n(\theta)$ and $Q_n(\theta)$ according to equations (84) and (85), respectively. With equations (105) and (106) we then obtain the recursion relations for these functions

$$(2n+1)p_n(\theta) = 2np_{n-1}(\theta) - |\cos\theta|(\sin^2\theta)^n, \tag{108}$$

$$(2n-1)q_n(\theta) = 2nq_{n-1}(\theta) + (\sin^2\theta)^n, \tag{109}$$

and the initial values are $p_0(\theta) = 1 - |\cos\theta|$ and $q_0(\theta) = |\cos\theta| - 1$. Values for special angles are

$$p_n(0) = q_n(0) = 0, \tag{110}$$

$$p_n(\pi/2) = \frac{4^n(n!)^2}{(2n+1)!}, \quad q_n(\pi/2) = -1. \tag{111}$$

Figure 9 shows the functions $p_n(\theta)$ and $q_n(\theta)$ for $n = 3$. With the recursion relations, the series for $M_k(\boldsymbol{q})^{ev}$ in equations (82) and (83) can be evaluated very efficiently. Figure 10 shows $M_e(\boldsymbol{q})^{ev}$ as a function of q for $\theta = 30°$, obtained by summing the series in equation (82) up to $n = 20$. We see from the graph that the series gives a perfect match with the exact result up to about $q = 20$, corresponding to a distance of about three wavelengths to the origin of coordinates. At this distance the uniform asymptotic expansion sets in, and in this sense both results are complementary.

13. New integral representations

With the results from the previous section we can derive some interesting new integral representations for the auxiliary functions. In this section we shall only consider $0 \le \theta \le \pi/2$, which will simplify the notation somewhat. Since the functions are reflection symmetric with respect to the xy-plane, this is no limitation. When we set $x = \cos\theta$ in equation (103) we find

$$P_n(\theta) = \frac{1}{\cos\theta} \int_0^{\cos\theta} dt \, (1 - t^2)^n, \tag{112}$$

and then we make the change of variables $t = \cos\alpha$, which yields

$$P_n(\theta) = \frac{1}{\cos\theta} \int_\theta^{\pi/2} d\alpha \, (\sin\alpha)^{2n+1}. \tag{113}$$

When we substitute this result in the series expansion (78), the summation over n is just the series expansion of the Bessel function of order 2, equation (53), and so we obtain

$$\mathrm{Re}M_f(\boldsymbol{q})^{tr} = -\sin\theta \int_\theta^{\pi/2} d\alpha \, \frac{1}{\sin\alpha} J_2(q\sin\alpha). \tag{114}$$

This remarkable result should be compared to the original integral representation (36), which is much more cumbersome in appearance. Interesting to notice is that the new integral representation involves a Bessel function of different order compared to the original integral representation.

Also the evanescent part allows a new integral representation. To this end, we notice that equation (102) can also be integrated as

$$Y_n(x) = Y_n(1) + \int_1^x dt \, (1 - t^2)^n, \tag{115}$$

instead as in equation (103). Then we put again $x = \cos\theta$, and with $Y_n(1) = P_n(0)$
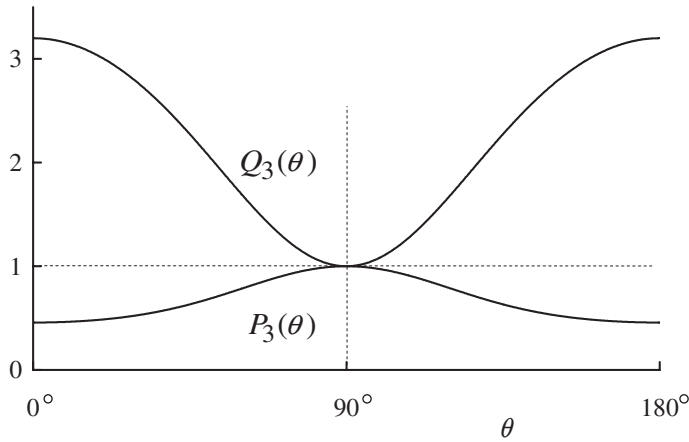
Figure 8.   Illustration of the coefficient functions for travelling waves.
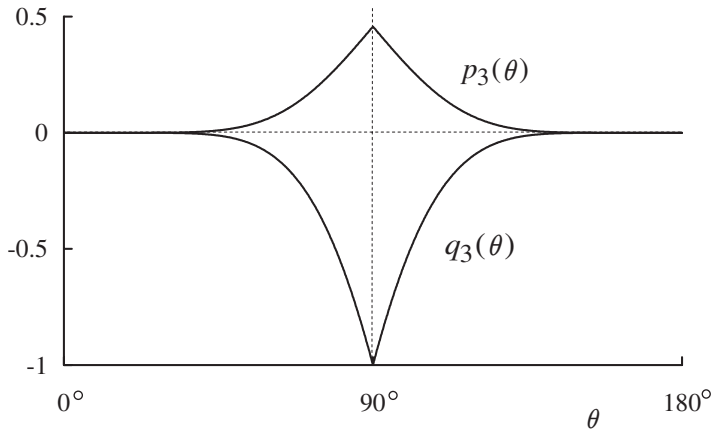
Figure 9.   Illustration of the coefficient functions for evanescent waves.

this gives

$$P_n(\theta) = \frac{1}{\cos\theta}\left[P_n(0) - \int_{\cos\theta}^{1} dt\,(1 - t^2)^n\right]. \tag{116}$$

When we compare this to definition (84) of $p_n(\theta)$, we see that this is just

$$p_n(\theta) = \int_{\cos\theta}^{1} dt\,(1 - t^2)^n. \tag{117}$$

Setting again $t = \cos\alpha$ gives

$$p_n(\theta) = \int_0^{\theta} d\alpha\,(\sin\alpha)^{2n+1}, \tag{118}$$
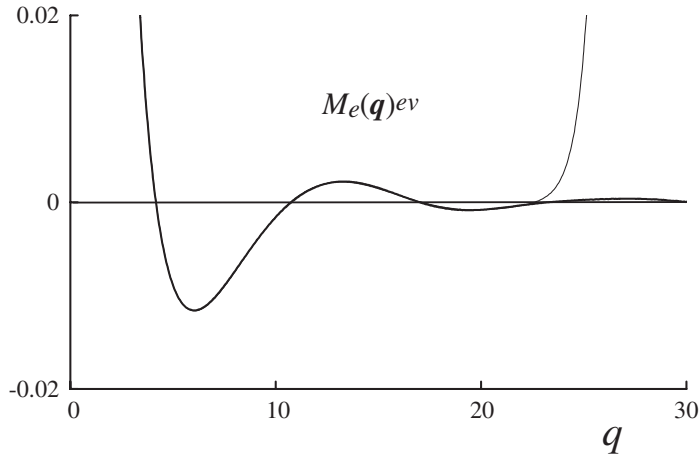
Figure 10. Exact value of $M_e(\boldsymbol{q})^{ev}$ (thick line) for $\theta = 30°$ and its series approximation from equation (82), summed up to $n = 20$ (thin line).

and when we substitute this in the series expansion (83), the sum is again a Bessel function. We then find

$$M_f(\boldsymbol{q})^{ev} = \sin\theta\left(\frac{1}{q^2} + \frac{1}{2}\right) - \sin\theta\int_0^\theta d\alpha\,\frac{1}{\sin\alpha}J_2(q\sin\alpha). \qquad (119)$$

Compared to the travelling part, equation (114), we notice that both integrals have the same integrands, and they only differ in their integration limits. When we add both integral representations we obtain

$$\mathrm{Re}M_f(\boldsymbol{q}) = \sin\theta\left(\frac{1}{q^2} + \frac{1}{2}\right) - \sin\theta\int_0^{\pi/2} d\alpha\,\frac{1}{\sin\alpha}J_2(q\sin\alpha), \qquad (120)$$

and this should be equal to the right-hand side of equation (33). The unsplit function $\mathrm{Re}M_f(\boldsymbol{q})$ contains a travelling and an evanescent contribution. When represented as in equation (120), the first term on the right-hand side is pure evanescent. When we split the integration range exactly at the polar angle θ of the field point, then the integral over $0 \le \alpha \le \theta$ gives the remaining evanescent part of this function, and the integral over $\theta \le \alpha \le \pi/2$ accounts for the travelling contribution. We have verified numerically that these new integral representations reproduce indeed $\mathrm{Re}M_f(\boldsymbol{q})^{tr}$ and $M_f(\boldsymbol{q})^{ev}$, obtained by numerical integration of the old representations.

The series expansions for $\mathrm{Re}M_e(\boldsymbol{q})^{tr}$ and $M_e(\boldsymbol{q})^{ev}$, as given by equations (77) and (82), respectively, involve the coefficient functions $Q_n(\theta)$ and $q_n(\theta)$. In order to derive integral representations for $Q_n(\theta)$ and $q_n(\theta)$ we introduce

$$Z_n(x) = \sum_{k=1}^n \binom{n}{k}\frac{(-1)^k}{2k-1}x^{2k-1}, \qquad (121)$$

in analogy to the function $Y_n(x)$ in equation (101), and from equation (100) we see that

$$Q_n(\theta) = 1 - \cos\theta Z_n(\cos\theta). \qquad (122)$$

It follows by inspection that $Z_n(x)$ satisfies the differential equation

$$\frac{dZ_n}{dx} = \frac{1}{x^2}\left[(1 - x^2)^n - 1\right], \qquad (123)$$

and with $Z_n(0) = 0$ this can be integrated as in equation (103). We then set $x = \cos\theta$, which gives

$$Q_n(\theta) = 1 + \cos\theta \int_0^{\cos\theta} dt \frac{1}{t^2}\left[1 - (1 - t^2)^n\right], \qquad (124)$$

and with the substitution $t = \cos\alpha$ this becomes

$$Q_n(\theta) = 1 + \cos\theta \int_\theta^{\pi/2} d\alpha \frac{\sin\alpha}{\cos^2\alpha}\left[1 - (\sin\alpha)^{2n}\right], \qquad (125)$$

in analogy to the representation (113) for $P_n(\theta)$.

We now substitute the representation (125) into the series representation (77), which gives the new integral representation

$$\mathrm{Re}M_e(\boldsymbol{q})^{tr} = \frac{1}{q}J_1(q) - \frac{1}{q}\cos\theta \int_\theta^{\pi/2} d\alpha \frac{1}{\cos^2\alpha}[J_1(q\sin\alpha) - \sin\alpha J_1(q)]. \qquad (126)$$

The appearance of this result is very similar to equation (114), with the exception that an additional term $J_1(q)/q$ appears. For $\theta = \pi/2$, the integral on the right-hand side of equation (126) vanishes, and only this term $J_1(q)/q$ remains. This is just the value of $\mathrm{Re}M_e(\boldsymbol{q})^{tr}$ in the xy-plane, as we already found in equation (48). It was also observed in section 7 that this term could be considered a result of the splitting, since $\mathrm{Re}M_e(\boldsymbol{q})$ itself is identically zero in the xy-plane.

For the evanescent part we need a representation for $q_n(\theta)$. Equation (124) is the integral of equation (123) around $x = 0$. When we integrate around $x = 1$ and use $Z_n(1) = 1 - Q_n(0)$ we find

$$Q_n(\theta) = \cos\theta\left[Q_n(0) + \int_{\cos\theta}^1 dt \frac{1}{t^2}(1 - t^2)^n\right], \qquad (127)$$

and with equation (85) this is

$$q_n(\theta) = -\cos\theta \int_{\cos\theta}^1 dt \frac{1}{t^2}(1 - t^2)^n. \qquad (128)$$

For $\theta \to \pi/2$ the integral does not converge in the lower limit, but the overall $\cos\theta$ keeps $q_n(\pi/2)$ finite, and equal to -1. With $t = \cos\alpha$, equation (128) becomes

$$q_n(\theta) = -\cos\theta \int_0^\theta d\alpha \frac{1}{\cos^2\alpha}(\sin\alpha)^{2n+1}, \qquad (129)$$

which we now substitute in the series representation (82). This gives

$$M_e(\boldsymbol{q})^{ev} = \frac{1}{q^2}\cos\theta - \frac{1}{q}\cos\theta \int_0^\theta d\alpha \frac{1}{\cos^2\alpha}J_1(q\sin\alpha). \qquad (130)$$

In this representation the integrand is not the same as in equation (126) for the travelling part. We can write equation (130) also as

$$M_e(\boldsymbol{q})^{ev} = \frac{1}{q^2}\cos\theta + \frac{1}{q}J_1(q)(\cos\theta - 1) - \frac{1}{q}\cos\theta \int_0^\theta d\alpha \, \frac{1}{\cos^2\alpha}[J_1(q\sin\alpha) - \sin\alpha J_1(q)],$$ (131)

and now the integrands are the same. When added to equation (126) we find

$$\text{Re}\,M_e(\boldsymbol{q}) = \left(\frac{1}{q}J_1(q) + \frac{1}{q^2}\right)\cos\theta - \frac{1}{q}\cos\theta \int_0^{\pi/2} d\alpha \, \frac{1}{\cos^2\alpha}[J_1(q\sin\alpha) - \sin\alpha J_1(q)],$$ (132)

and this should be equal to the right-hand side of equation (32). Here we see again that the integral over $0 \le \alpha \le \theta$ gives the evanescent contribution and the integral over $\theta \le \alpha \le \pi/2$ is the travelling part. The additional term on the right-hand side is pure evanescent. In addition, the travelling part gets a term $J_1(q)/q$ and the evanescent part a term $-J_1(q)/q$. In the sum, equation (132), these terms have canceled. In this sense we can consider the appearance of the terms $\pm J_1(q)/q$ a result of the splitting, as mentioned in section 7.

14. Conclusions

We have studied the travelling and evanescent waves in the magnetic field of an electric dipole. In an angular spectrum representation of the magnetic field, both parts appear as integrals over the $\boldsymbol{k}_{\|}$-plane. The integration over the azimuthal angle can be performed in closed form, leading to Bessel functions. Rather than considering the magnetic field itself, we have introduced a Green's vector which determines the magnetic field in a simple way, and which contains all spatial dependence of the field. In this fashion, the approach is independent of the orientation of the dipole. This Green's vector was expressed in terms of two auxiliary functions, which both have a travelling and an evanescent part. The imaginary parts of these functions are known in closed form, and only have a travelling part. Therefore we only had to consider the splitting of the real parts of the auxiliary functions into their travelling and evanescent contributions.

We have obtained full asymptotic series, for $|\bar{z}|$ large, for the evanescent parts of both the auxiliary functions. It followed that in most of space the behaviour of the evanescent waves is $\mathcal{O}(q^{-3/2})$, indicating that the evanescent waves die out with distance faster than $\mathcal{O}(q^{-1})$, and therefore do not contribute the far field. This in contrast to the evanescent part of the electric field, which survives in the far field in a small cylinder around the z-axis. In order to include the behaviour in the neighbourhood of the xy-plane we have obtained a uniform asymptotic approximation which holds for all angles θ. By considering $\theta \to \pi/2$ we found that near the xy-plane the evanescent waves do survive in the far field as $\mathcal{O}(q^{-1})$, just as the evanescent part of the electric field.

For the study of the near field we have first obtained series expansions in $\bar{z}$, for $\bar{z}$ small, of the travelling parts of the auxiliary functions. These series were then converted into series in the radial distance q, with the coefficients functions of the polar angle θ. From these series we have derived similar series for the evanescent

parts of the auxiliary functions. It was shown that all singular terms in the magnetic field are entirely due to the evanescent waves, and they appear as separate terms in the series expansions. From the properties of the coefficient functions in the series expansions in q we have derived interesting new integral representations for the travelling and evanescent parts of the auxiliary functions.

References

[1] F. de Fornel, *Evanescent Waves. From Newtonian Optics to Atomic Optics* (Springer-Verlag, Berlin, 2001).
[2] G.A. Massey, Appl. Opt. **23** 658 (1984).
[3] J.M. Vigoureux, F. Depasse and G. Girard, Appl. Opt. **31** 3036 (1992).
[4] D.W. Pohl, In *Advances in Optical and Electron Microscopy*, edited by T. Mulvey and C.J.R. Sheppard (Academic Press, San Diego, 1991), p. 243.
[5] D.W. Pohl and D. Courjon (Editors), *Near Field Optics*, Proc. of the NATO Advanced Research Workshop on Near Field Optics, Series E, Applied Sciences, Vol. 242 (Kluwer, Dordrecht, 1993).
[6] D. Courjon and C. Bainier, Rep. Prog. Phys. **57** 989 (1994).
[7] M.A. Paesler and P.J. Moyer, *Near Field Optics, Theory, Instrumentation, and Applications* (Wiley, New York, 1996).
[8] M. Ohtsu (Editor) *Near-Field Nano/Atom Optics and Technology* (Springer-Verlag, Berlin, 1998).
[9] K.T.V. Grattan and B.T. Meggitt (Editors), *Optical Fiber Sensor Technology, Fundamentals* (Kluwer, Dordrecht, The Netherlands, 2000).
[10] D. Courjon, *Near-Field Microscopy and Near-Field Optics* (World Scientific, Singapore, 2003).
[11] L. Novotny, D.W. Pohl and P. Regli, J. Opt. Soc. Am. A **11** 1768 (1994).
[12] B. Hecht, H. Bielefeldt, D.W. Pohl, *et al.*, J. Appl. Phys. **84** 5873 (1998).
[13] C.K. Carniglia, L. Mandel and K.H. Drexhage, J. Opt. Soc. Am. **62** 479 (1972).
[14] D. van Labeke, F. Baida, D. Barchiesi and D. Courjon, Opt. Commun. **114** 470 (1995).
[15] D. van Labeke, D. Barchiesi and F. Baida, J. Opt. Soc. Am. A **12** 695 (1995).
[16] B. Hecht, D.W. Pohl, H. Heinzelmann, *et al.*, In *Photons and Local Probes*, edited by O. Marti and R. Möller (Kluwer, Dordrecht, 1995), pp. 93–107.
[17] H. Heinzelmann, B. Hecht, L. Novotny, *et al.*, J. Micr. **177** 115 (1995).
[18] B. Hecht, Forbidden light scanning near-field optical microscopy. Thesis, University of Basel, Switzerland (1996).
[19] H.F. Arnoldus and J.T. Foley, Opt. Lett. **28** 1299 (2003).
[20] H.F. Arnoldus and J.T. Foley, J. Opt. Soc. Am. A **21** 1109 (2004).
[21] E. Wolf and J.T. Foley, Opt. Lett. **23** 16 (1998).
[22] A.V. Shchegrov and P.S. Carney, J. Opt. Soc. Am. A **16** 2583 (1999).
[23] T. Setälä, M. Kaivola and A.T. Friberg, Phys. Rev. E **59** 1200 (1999).
[24] H.F. Arnoldus and J.T. Foley, J. Opt. Soc. Am. A **19** 1701 (2002).
[25] M.V. Berry, J. Mod. Opt. **48** 1535 (2001).
[26] H.F. Arnoldus and J.T. Foley, Opt. Commun. **207** 7 (2002).
[27] C.T. Tai, *Dyadic Green's Functions in Electromagnetic Theory* (Intext, Scranton, 1971), p. 55.
[28] J. van Kranendonk and J.E. Sipe, In *Progress in Optics*, Vol. XV, edited by E. Wolf (North-Holland, Amsterdam, 1977), pp. 246–350.
[29] J. van Bladel, *Singular Electromagnetic Fields and Sources* (Clarendon Press, Oxford, 1991), p. 91.
[30] L. Mandel and E. Wolf, *Optical Coherence and Quantum Optics*, Section 3.2.4 (Cambridge University Press, Cambridge, 1995).
[31] D.G. Duffy, *Green's Functions with Applications, Studies in Advanced Mathematics* (Chapman & Hall/CRC, Boca Raton, 2001), p. 104.
[32] H.F. Arnoldus and J.T. Foley, J. Mod. Opt. **50** 1883 (2003).

[33] F.W.J. Olver, *Asymptotics and Special Functions* (Academic Press, New York, 1974), p. 344.
[34] N. Bleistein and R.A. Handelsman, *Asymptotic Expansions of Integrals* (Dover, New York, 1986), p. 380.
[35] R. Wong, *Asymptotic Approximations of Integrals* (Academic Press, Boston, 1989), p. 410.
[36] M. Abramowitz and I. Stegun, *Handbook of Mathematical Functions* (Dover, New York, 1972), p. 298.
[37] A.P. Prudnikov, Yu. A. Brychkov and O.I. Marichev, *Integrals and Series*, Vol. 1, Elementary Functions (Gordon and Breach, New York, 1986), p. 710.